Style-of-faulting of expected earthquakes in Italy as an input for seismic hazard modeling

5   S. Pondrelli[1], F. Visini[2], A. Rovida[3],V. D'Amico[2], B. Pace[4] and C. Meletti[2],

(1) Istituto Nazionale di Geofisica e Vulcanologia, Sezione di Bologna, Italy,
(2) Istituto Nazionale di Geofisica e Vulcanologia, Sezione di Pisa, Italy,
(3) Istituto Nazionale di Geofisica e Vulcanologia, Sezione di Milano, Italy,
10   (4) DiSPUTer Department, Università G. d'Annunzio Chieti-Pescara, Chieti, Italy

Abstract

15   The style-of-faulting and distributions of nodal planes are an essential input for probabilistic seismic hazard assessment. As a part of a recent elaboration of a new seismic hazard model for Italy, we defined criteria to parametrize the style-of-faulting of expected earthquake ruptures and evaluate their representativeness in an area-based seismicity model. Using available seismic moment tensors for relevant seismic events (Mw ≥ 4.5), first
20   arrival focal mechanisms for less recent earthquakes and also geological data on past activated faults, we collected a database for the last ~100 yrs, gathering a thousand of data all over the Italian peninsula and regions around it. On this dataset we adopted a procedure that consists, in each seismic zone, of separating the available seismic moment tensors in the three main tectonic styles, making summation within each group, identifying possible
25   nodal plane(s), taking into account the different percentages of style-of-faulting and including, where necessary, total or partial (even in terms of tectonic style) random source contributions. Referring to the used area source model, for several seismic zones we obtained robust results, e.g. along the central and southern Apennines we expect future earthquakes to be mostly extensional, although in the outer part of the chain reverse and
30   strike-slip events are possible. In the Northern part of the Apennines we expect different style-of-faulting for different hypocentral depths. In zones characterized by a low seismic moment release, the possible style-of-faulting of future earthquakes is less clear and it has been represented using different combination of random sources.

35   ## Introduction

The determination of the style-of-faulting in seismicity models for Probabilistic Seismic Hazard Assessment (PSHA) represents the key ingredient to define the orientation and the kinematics of the seismic source. The orientation, i.e, strike and dip, impacts the source-to-
40   site distance whereas the kinematics, i.e. the rake, is linked to the choice of the coefficients of the Ground Motion Prediction Equations (GMPE), that take into account the style-of-faulting. The comparison of ground motions produced by reverse, strike-slip or normal faults shows that reverse-faulting events generate higher amplitude motions, especially with respect to normal faulting ones (e.g. Bommer, 2003). According to Bindi et al. (2011), in the
45   case of the Italian strong motion data, the main differences in the ground motion result over the medium-to-short period range (T<1 s), where the expected values for a reverse mechanism are significantly larger than those produced by the other styles of faulting. As concerns the source orientation, changing the strike of the fault leads to an increment/

reduction of the rupture-to-site distance. For instance, in the case of a normal fault with Mw 6.3, the GMPE by Bindi et al. (2011) shows that increasing the distance from 20 to 30 km reduces the mean expected Peak Ground Acceleration (PGA) of about 40%.

Although orientation and kinematics of the finite ruptures are a key ingredient for PSHA, there are no standard objective approaches for defining the style-of-faulting in tectonic regions, and this is generally reminded as an analysis of available fault mechanisms and a comparison with mapped active faults. Roselli et al. (2017) defined the style-of-faulting on a regular grid in Italy. They used a smoothed 2D approach started from the computation, for each cell, of a cumulative focal mechanism obtained with a weighted summation of previous focal mechanisms. However, in general, the lack of a seismotectonic model behind the calculation can affect the results, especially in small areas characterised by the coexistence of normal, reverse, and strike slip tectonics. In addition the variation of each style-of-faulting with depth should be detected and taken into account where possible.

Our objective is to define an approach based on seismotectonic zones, because it allows including possible variability in the style-of-faulting with depth and preventing undesired rotations of average focal solution in case of transitions to different kinematics at the surface or at depth. Meletti et al. (2017) released a seismogenic zone model, named ZS16, that represents the update of the ZS9 model (Meletti et al., 2008) adopted by the current reference seismic hazard model of Italy (Stucchi et al., 2011). ZS16 is based on the same seismotectonic knowledge used for designing ZS9, but includes many new data available for the study area (earthquake catalog and fault database among others) that allow a better definition of the boundary and of the seismogenic depth of each seismic source zone.

In this paper we illustrate the selection and weighting criteria to gather a representative dataset of nearly 100 years of focal mechanisms in Italy, and the procedure we tested and applied to define the style-of-faulting using the recently produced ZS16 seismotectonic zoning for the update of the national PSHA for Italy.

Seismotectonic framework and seismogenic zones

The seismotectonic setting of Italy shows the presence of all tectonic styles: normal, compressive, strike slip and the combination of them (Figure 1). In the Alps, the most seismically active part is the eastern one, where the south verging Alpine thrusts meet the strike slip Dinaric structures, and where the famous 1976 Friuli seismic sequence included several great to moderate earthquakes with reverse and strike-slip focal mechanisms (Pondrelli et al., 2001). Moving towards the south, along the entire Apennines watershed, a shallow extensional tectonics dominates, as testified also by the seismic sequences of 1997-1998 Umbria-Marche, of L'Aquila 2009 and the recent 2016-2017 Central Italy (Figure 1; Chiarabba et al., 2018 and references therein). This normal tectonic style continues up to the Calabrian Arc and in N-NE Sicily. However, on the outer part of the chain, on the Adriatic side, compressive tectonic occurs in correspondence with the northern Apennine arc, and the 2012 Emilia seismic sequence was its most recent expression (Anzidei et al., 2012). To the south, tectonics becomes strike slip to transpressive in correspondence of the outer part of the southern Apennines, i.e. in the Gargano Promontory (Figure 1). Another characteristic of the seismicity of the Adriatic side of the peninsula is a general greater hypocentral depth of the earthquakes, so to have not only a lateral variation of the dominating tectonic style, but also with depth. Crossing the Messina strait, that separates Calabria from Sicily, we still find a shallow extensional seismicity along the mountains watershed, that is however a less

persistent feature. In fact in Sicily other tectonic styles prevail, as for instance the north-south narrow bend from Aeolian islands up to the south of Mt. Etna, which is densely populated by strike-slip earthquakes, or the active compressive front west of the Aeolian islands, offshore northern Sicily in the southern Tyrrhenian Sea (Figure 1). This quick overview of the seismotectonic characteristics of the Italian peninsula is based on seismological and geological data, strictly related to what happens at crustal depth and thickness; in fact the subduction system and related deep seismicity active beneath the Calabrian arc and the southern Tyrrhenian sea is here excluded because we focus on shallow seismicity responsible for seismic hazard.

Meletti et al. (2019) defined a seismotectonic zoning, named ZS16, reflecting the structural tectonic framework of Italy, that we adopt for our study. It is composed of 50 area sources representing regions of spatially uniform occurrence of seismicity (Figure 1 and Table S1). To define the borders of the zones, and the upper and lower bounds of the characteristic seismogenic depth, data from mapped active faults (DISS Working Group, 2018), that played a major role, have been integrated with earthquake catalogues (Rovida et al., 2016), geodetic strain data (Devoti et al., 2016) and focal mechanisms (Global CMT, Ekström et al., 2002; European Mediterranean RCMT Catalog, 2020). In order to estimate the upper and lower seismogenic depths of the ZS16 zones for the earthquakes above the threshold relevant for the PSHA, the instrumental catalogue prepared for the recent elaboration of a new seismic hazard model for Italy (MPS19 Project) has been used (Gasperini et al., 2016). Earthquakes with fixed depth have been removed from the reference dataset; only earthquakes that likely occurred within shallow crust, with a maximum depth of 40 km, have been included. The 5th and 95th percentile of the cumulative depth distribution of the selected dataset have been assumed as the upper and lower boundaries of the seismogenic layer depth. Finally, the definition of the upper and lower depths is reached comparing the percentiles resulting from catalogues with different minimum magnitudes (from Mw 2 to Mw 4) with the depth of the composite seismogenic sources from DISS 3.2.1. In Table S1 the obtained depth values used in ZS16 for the 50 area sources are listed

Data and Methods

Here we describe the building of the focal mechanism database and the procedure applied to evaluate the prevailing style-of-faulting.

Data

To collect the representative dataset useful to define the different seismotectonic styles for the Italian peninsula, we started from the best quality moment tensors available, that is the CMT Italian Dataset (CMT Italian Dataset, 2020; Pondrelli et al., 2006). It is a continuously updated merge of the existing Global CMTs (Dziewonski et al., 1981; Ekström et al., 2012) and European-Mediterranean RCMT data (European Mediterranean RCMT Catalog, 2020; Pondrelli et al., 2002; Pondrelli and Salimbeni, 2015, including all moment tensors available for earthquakes with M≥4.5 in the time interval from 1976 to 2015 included in the geographical window with latitude from 35° to 48°N and longitude from 6° to 20°E. To reach the best homogeneity in terms of spatial distribution, we added the moment tensors of a few M≥4.0 earthquakes occurred in the Alpine region, obtained by seismic data inversions and belonging to the GFZ and ETHZ datasets (Saul et al., 2011 and Bernardi et al., 2004 respectively).

145　To get a longer dataset in terms of time, we considered also first polarities focal solutions selected from the EMMA Database (Database of Earthquake Mechanisms of the Mediterranean Area, Vannucci and Gasperini, 2004). Such data have been used when they were the only available ones, thus for the relevant events occurred before the digital era of seismological data, as for instance the 1968 Belice (Sicily) earthquakes. In a few cases,

150　multiple focal mechanisms are available for a single event. To choose among them we applied the quality evaluation given in the EMMA Database selecting the so-called "preferred" solutions.

However, for two great events of the past century, the 1905 M6.9 in Calabria and the 1915 M6.9 in the Southern Apennines, several first arrival focal mechanisms available in the

155　EMMA Database are available, unfortunately of low quality and different from one to another, indicating a different tectonic style from that expected in the regions where they occured. For both earthquakes, none of the "preferred" nearly strike-slip solutions was considered reliable enough because the strike slip kinematic seems far to be compatible with the crustal tectonic style of the Southern Apennines and Calabria regions, usually described as extensional (e.g.

160　D'Agostino et al., 2011).

Considering the high magnitude of these events and the aim of this study, we decided to look for different data to reconstruct their focal mechanisms. To do so we took into account the following statements: 1) first arrival focal mechanisms are often different from seismic moment tensor focal mechanisms (see the astonishing example of the M 6.0 Amatrice

165　earthquake, Central Italy, August 24 2016 of Figure 2 in Marchetti et al., 2016); 2) first arrival focal mechanisms represent the initial fault slip, while seismic moment tensors describe the entire seismic source, which in turn is considered the most representative indicator of the tectonic style dominating the epicentral region.

Our attention thus went to Quaternary tectonics information in the DISS database (DISS

170　Working Group, 2018), according to which the seismogenic sources of both events are described as pure extensional, based on geological studies (e.g. Loreto et al., 2013 for the 1905 Calabria earthquake; Galadini and Galli, 1999 for the 1915 earthquake). Thus, for the 1905 earthquake we used a seismic moment tensor reconstructed using the strike, dip and rake given in the seismogenic source ITIS139, Sant'Eufemia Individual Source, and for the

175　1915 those given in the ITIS002, Fucino Basin Individual Source. It is worth noting that from DISS we exported only the strike, slip and rake reported in the parameters lists, while for magnitude and seismic moment we kept those from the "preferred" solution in the EMMA database, because determined with seismological recordings, as all other similar data of our dataset.

180　The final database (Figure 1 and Table S2 in the Supplementary Material) includes nearly 1000 focal mechanisms for crustal earthquakes, representative of about 100 years of seismicity of the Italian peninsula and surrounding areas.

We are aware that for some regions the possible largest earthquake could be not represented in the available observations. Looking for the prevailing style-of-faulting, we

185　needed information on the focal mechanism of events, which of course do not exist for great earthquakes of the past. This lack of knowledge should be taken into account together with other uncertainties when the results of this work will be used in hazard model computations, as well as it is done for data from historical catalogs, where it is known that ancient big earthquakes may lack. By the way, considering how long geological process last, we

190　assume that where we have focal mechanisms for recent events coherent with geological structures, they may be considered representative of historical earthquakes, too.

Methods

195 Several ground motion prediction equations include the "style-of-faulting" as a possible variable (e.g. Bindi et al., 2011; Akkar et al., 2014; Bindi et al., 2014) and the modern seismic hazard softwares (e.g. OpenQuake Engine, Pagani et al., 2014) need the prevalent fault geometry of the expected ruptures to be used for the source definition. However, because the style-of-faulting impacts the PSHA in an area, it is important to define when the
200 calculated style-of-faulting can be considered robust and representative of the kinematics of a region.

We started firstly applying a traditional Kostrov's method (Kostrov, 1974), in which the sum of the moment tensor elements M_{ij} is taken for all of the N_{ev} earthquakes located within the volume V, obtaining a cumulative seismic moment tensor representative of the seismic
205 deformation occurred within V. This method can be applied to every volume, i.e. each seismic zone, for which earthquake moment tensors are available, that in our study means 41 of the 50 source areas (Table 1). In 5 of the remaining 9 areas, the summation cannot be done because no events with M≥ 4.5 are present, while the other 4 areas have only one earthquake within the considered magnitude range (Table 1).
210 A sensitive parameter is the depth of seismogenic layer we use in the summation for each zone. We already have indications from the values attributed to ZS16 seismic zones, but we also know that in some regions a change in the tectonic style with depth may occur, so we perform one test to find the most appropriate values.

We calculated the cumulative seismic moment tensors assuming different thicknesses of the
215 volume V, equal for all zones, respectively of 10, 20 and 30 km (an example in Figure 2). Comparing the results, we observed that in some zones the cumulative moment tensors are different when calculated using different thickness. An example is given by zone n. 19 in the Northern Apennines, where a seismogenic layer of 10 km of thickness shows a purely extensional cumulative seismic moment tensor (Figure 3), while a summation over a layer of
220 20 km produces a transpressive focal mechanism. The distribution with depth of focal mechanism style of this part of the Apennines in fact shows a prevailing presence of extensional earthquakes in the shallower part of the crust while, moving E-NE, beneath normal sources, reverse and strike slip focal mechanisms are the most frequent (see Section in Figure 3). We defined schematically this behavior as a "tectonic layering", and where we
225 detected it, in the three seismic zones n. 19, 20 and 25, we proceed with a summation over two different layers, with thickness depending on the local seismicity distribution with depth (Table 1). For all the other zones, we used a 40 km thickness for conservative reasons to make sure the inclusion of all selected seismic events in our computation.

These summation tests allowed also to investigate if the summed solutions were
230 representative of the kinematics of each zone, and how the input dataset influences the robustness of the results. When the cumulative moment tensors were obtained summing data for $N_{ev} \geq 3$ and the input dataset was homogeneous as concerns the tectonic style, the results were consistent with the tectonics of the region and thus considered representative (red focal mechanisms in Figure 2). A good example is given by the Eastern Alpine region,
235 where for seismic zones 1, 2 and 3, reverse and strike-slip cumulative focal mechanisms well reflect the compressive active tectonic of Southern Alps and the strike-slip deformation which prevails to the east in the Dinaric chain. On the contrary, when the cumulative moment tensor was the sum of three or less moment tensors (yellow focal mechanisms in Figure 2), or it was obtained with more than three earthquakes, but with the summation of a
240 heterogeneous dataset (light blue focal mechanisms in Figure 2), i.e. several focal

mechanisms with different tectonic styles and/or very different directions of strike, dip and rake, we considered the results insufficiently representative. This last case occurs mainly in seismic zones characterized by small to moderate magnitude earthquakes, or including seismotectonic structures with different orientations. An example is the area source n. 11,

245 which contains part of western Alps and the western Po Plain (Figure 2), where most of available focal mechanisms are strike slip, but with very different and scattered directions of the focal planes.

To reduce the amount of such unreliable results, that affect nearly half of the seismic zones, we implemented the following methodology. In each seismic zone we splitted the entire

250 dataset in the three main tectonic styles, following the rake-based criteria given in Akkar et al. (2014) which attribute each focal mechanism to a specific kinematics, reverse, normal or strike-slip. In particular, normal solutions have a rake between -135° and -45°, reverse solutions between 45° and 135°, other rake values are classified as strike slip.

We then applied the Kostrov summation over each homogenous — from the tectonic point of

255 view — group of moment tensors having more than one earthquake. In Table 1 the results for each zone are reported (cumulative M_0, strike, dip and rake of the cumulative focal mechanism for each tectonic style).

We computed also the dispersion of the P-, T- and B- axes of the input focal mechanisms with respect to the position of the P-, T- and B- axes of the cumulative moment tensor (Table

260 2). For example, as reported in Figure 4, in the source area n. 9 we have 7 input data; we computed the angular distance between the P- T- and B- axes (red and blue points in Figure 4a) and the axes of the cumulative focal mechanism (green symbols in Figure 4a). The three median values of the angular distances of the three axes are a measure of how much dispersed and heterogeneous are the input data, and consequently of the robustness of the

265 obtained nodal plane distribution. The three median values are then used as a weighting factor for defining the final style of faulting for each zone.

To identify the representative style-of-faulting for each source zone, we used a procedure based on the following parameters:

270 ➢ N_{ev}, the number of available focal mechanisms for each zone and for each tectonic style,

➢ M_{0sum}, the seismic moment obtained from the summation for each zone and tectonic style; in particular its percentage with respect to the M_{0Total}, the total seismic moment for each seismic zone independently by the tectonic style (Table 3)

275 ➢ the median of the angular distance between P-, T-, B- axes (Table 2), as a measure of data input dispersion.

The value of these parameters has been used to apply the following decision-making process, also sketched in Figure 5:

280 a) in areas where no focal planes at all were available, we parameterized the less informative solution, given by a equal contributions of normal, reverse and strike-slip tectonic styles, and by adopting a uniform distribution of geometries (strike and dip) in the space, defining a 100% random source;

b) if more than one event of the same tectonic style is located in an area, we identified the

285 nodal planes and their contributions in terms of seismic moment M_0. As a first step we summed the seismic moment tensors to obtain M_{0sum} and a cumulative moment tensor, then we apply the following criteria:

- if M_{0sum} for a particular tectonic style is lower than the 10% of M_{0Total} of the zone, we

do not take into account that tectonic style in the final solution. For example, in the zone n. 39 , the strike-slip component is not included in the final result (Tables 1 and 3);

- if M_{0sum} of a single tectonic style is greater than the 10% of M_{0Total} of the zone, but the number of summed earthquakes is lower than 3, we kept this tectonic style in the final seismic source by adopting a uniform distribution of geometries (strike-dip) in the space with a fixed rake, also defined as a random component. An example is the zone n. 12 (Tables 1 and 3), where the compressive contribution is included, defined as TFrandom, but modelled without preferred fault planes;

- for each tectonic style of the zones with a contribution in M_{0sum} greater than the 10% of M_{0Total} and obtained with a number of earthquakes greater than 2, we measure the dispersion of the P-, T- and B- axes of the input focal mechanisms with respect to those of the cumulative moment tensor: if 2 or more of the three axes have the median of the angular differences greater than 30° (Table 2), we include this tectonic style, but adopting a uniform distribution of geometries (random strike and dip) in the space with a fixed rake. An example is given by zone n. 9 where all data are strike-slip, but the analysis of P-, T- and B- axes distributions shows a dispersion larger than 30° for two of three axes (Figure 4) and the final style-of-faulting is 100% strike-slip random;

- if the M_{0sum} of a single tectonic style is greater than the 10% of the M_{0Total}, obtained with a number of events greater than 2, and with the maximum of the median of the angular distances of P-, T- and B- axes greater than 30°, it contributes to the final solution proportionally to its percentage with respect to the M_{0Total}. Moreover, the final focal mechanism is given by the cumulative one obtained by the Kostrov summation of available moment tensors of the single tectonic styles. An example is given by zone n. 43, where the final style-of-faulting is represented by a 45% of reverse source and 55% of a strike-slip; strike, dip and rake values reported in Table 3 for these final solutions originate from the cumulative moment tensors obtained summing respectively reverse and strike-slip input focal mechanisms.

Applying this decision making process to all seismic zones, we defined an expected style-of-faulting for all of them, reported in Table 3 and in Figure 6.

Results

In Figure 6 and Table 3 the results of the applied decision making process are shown. The variety of symbols and colors of Figure 6 represents the complexity of the seismotectonics of the Italian peninsula, and the attempt we made at taking all of them into account, encountering all possible cases between the 100% single tectonic style source to the 100% random source.

In only 15 zones the resulting focal solution is 100% of a single tectonic style, and often this occurs where great earthquakes are located, as in zone n. 33 which includes the 1980 Irpinia M 6.9 event. On the other hand, in 10 seismic areas the final source is 100% random, due to the lack or scarcity of seismic events with M ≥ 4.5, as for instance the zones n. 27 or 31 along the Tyrrhenian coast or the n. 37 and 38, offshore southern Puglia.

In several zones the final style-of-faulting is a partitioning between more than one tectonic style, with contributions defined by the percentage of the seismic moment M_{0sum} of each tectonic style. For instance, in the seismic zone n. 30 (Central Adriatic Sea), the tectonic
340 style of the final seismic source is 80% compressive and 20% strike-slip. A 5% of normal style is excluded because it does not reach the 10% threshold (Figure 5).

In some zones, the final style-of-faulting has a percentage of uniform distribution of geometries (strike-dip) in the space, that for the sake of simplicity we defined as a random component, namely NFrandom, TFrandom or SSrandom (Table 3). This means that when a
345 tectonic style can be used only as a constraint, a proper fix rake is adopted. In the seismic area n. 29 we defined a final style-of-faulting composed by 80% of reverse tectonic type and 20% of random strike-slip, i.e. a strike-slip mechanism with uniformly distributed value for strike and dip and a fixed rake.

Another case is represented by zones where the final source is given by different
350 percentages of more than one tectonic style, all random. For instance, in zone n. 40, the Ionian Sea side of the Calabria region, the final result is a combination of 15% extensional random and 85% strike-slip random. These kinds of results occur mainly where the input dataset shows a large dispersion and heterogeneity in input focal plane directions. For instance, in the NW of Italy, in the seismic zones n. 9, 10 and 11 (Table 3), the final style-of-
355 faulting we propose is a uniform distribution of strike-slip geometries, derived from several earthquakes located in the area, mostly strike-slip, but without any prevailing direction for the strike of focal planes.

A   tectonic layering has been identified in three seismic zones, n.19, 20 and 25, so we defined a style-of-faulting for both a shallow and a deep seismogenic layer (the latter,
360 represented in Figure 6 with focal mechanisms with a grey background or with circles with darker colours). The seismic zone n. 19s, for instance, has a final source composed by a 50% normal, 35% strike-slip and 15% compressive random; the final result for the deep layer (19d in Table 3, hypocentral depth between 15 and 40 km) is a 100% reverse style-of-faulting.
365

Discussion

We propose a set of criteria to select focal mechanisms for the definition of the style-of-faulting in area source models, and we apply them to the ZS16 seismotectonic zoning
370 (Meletti et al., 2019). Results are shown in figure 6 and listed in Table 3. We are confident in our results for several reasons.

The first is that the style-of-faulting defined for each zone using our decision-making process are strongly in agreement with other geological (DISS Working Group, 2018) and geodetic data (Serpelloni et al., 2005; D'Agostino et al., 2011). For instance, the normal tectonics that
375 characterizes the Apennines is confirmed in all the seismic zones that concern the highest part of the belt. The normal tectonic style changes to compressive and/or strike-slip moving toward the Adriatic side or going at depth; two of the three zones where a variation of the tectonic style with depth has been detected, show a prevailing extensional regime at shallow depth and a deeper reverse and/or strike-slip tectonic type. For the Alpine region, the
380 western part of the belt presents more uncertain results due to the characteristics of the seismicity, usually characterized by small to moderate magnitude; in the Eastern Alps our results are completely in agreement with the active deformation field, with compressive to transpressive tectonics of the Southern Alps and Dinarides.

385   A second reason that supports the reliability of our analysis is the comparison with the results given by Roselli et al. (2017), who used a different approach. Roselli et al. (2017) smoothed their dataset over a regular 0.1° grid and did not take into account the possible variability of the prevailing tectonic styles with depth. From a qualitative point of view, we observed a general agreement between our results, with major differences along the

390   boundary between areas that in Roselli et al. (2017) are characterized by lateral changes of tectonic regimes. It is worth noting that these are the regions where we detected a variation of the style-of-faulting with depth and so where we used a 3D approach. For instance in the Northern Apennines we obtain different, even opposite, style-of-faulting at different depths, as in zone n. 19, where the shallow solution is mainly normal type while at depth is a reverse

395   type. However, at the same time lateral variation in our results is smoothed and not related to the presence of a boundary, like the one between two seismic zones. Modelling the earthquake occurrence in this region, the definition of the hypocentral depth makes the difference; if we model a seismic event deeper than 15 km beneath zones 19 or 20, we should assume a mainly reverse style-of-faulting, and so a GMPE different from the one to

400   be used if the earthquake was shallower, i.e with a normal style-of-faulting.

    To further evaluate when our results are reliable indicators of the style-of-faulting of expected earthquakes we compared them with recent earthquakes. Indeed, the input dataset includes only events before 2015. So, all the seismicity recorded afterwards,

405   including the 2016-2017 Central Italy seismic sequence, can be used for a comparison test. Selecting from the INGV Italian Seismological Instrumental and Parametric Data-Base (ISIDe Working Group, 2007) all shallow earthquakes (within 40 km of hypocentral depth) with M ≥ 4.5 occurred between January 2016 and August 2019, we obtain the list of earthquakes reported in Table 4. We also included 4 events with M from 4.2 to 4.4 to

410   increase the case studies. For all these recent earthquakes, the corresponding seismic moment tensors have been extracted from the European Mediterranean RCMT Catalog (Figure 7). For earthquakes belonging to the Central Italy seismic sequence, we selected the largest ones only: the August 24, 2016, Mw 6.0, the October 30, Mw 6.5 and the January 18, 2017, Mw 5.5. Starting from them, all with an extensional moment tensor, it is evident the

415   agreement with the style-of-faulting defined for the seismic zone n. 24, where the expected source tectonic style is 100% normal (Figure 7C). Proceeding in the comparison, another correspondence is found in the Northern Apennines, where an event located below 15 km of hypocentral depth (Figure 7A, event n.6 in Table 4), thus in the lower layer of seismic zone n.19, shows a good similarity with the style-of-faulting defined for the area. A good

420   agreement is found for the event located at the border of the seismic zone n. 21, where expected and observed style-of-faulting are both pure reverse (Figure 7A, event n. 12 in Table 4). The same applies to the two strike-slip events occurred in the summer of 2018 in the seismic zone n.34, both showing a strong coherence with the expected style-of-faulting (Figure 7C, events n. 8 and 9 in Table 4). In Sicily, all recent earthquakes show a strike-slip

425   focal mechanism, in agreement with our results (Figure 7B, map below).
    In conclusion, recent earthquakes positively test our results, also in sources obtained following the choice to allow a 3D approach where necessary, as in the Northern Apennines.

Conclusions

430

    The methodology we proposed to calculate the style-of-faulting in a seismic zone model is based on the selection of input data (focal mechanisms) aimed to ensure: (i)

representativeness of the observed kinematics expected to occur in the future; (ii) summation of focal mechanisms representative of similar style-of-faulting; (iii) the control of the dispersion of the nodal planes before their summation with respect to the cumulative one. Finally, the here described procedure can be exported to any area source based model, as it represents a data-driven approach, with subjectivity restrained to define threshold for dispersions of the input focal mechanisms.

Ultimately, we defined the tectonic style-of-faulting of possible expected earthquakes for each seismic zone of the seismogenic area source model ZS16 (Meletti et al., 2019).

In Figure 6, the final results map, the various symbols we had to use reflect all the different situations we detected and mirror the seismotectonic complexities we took into account even on a simplified seismic zones model. On a general view, in the Alps a compressive regime is found in the eastern part of the belt (zones n. 1, 2, 3), mixed in a different percentage with a strike-slip style-of-faulting moving toward the Dinaric chain to east. The rest of the Alps shows examples of all the possible style-of-faultings with also all the different percentages of random sources, sometime 100% random (e.g. zones n. 6, 8, 14), sometime a combination of different amounts of single tectonic style random sources (e.g. zone n. 11), and this is due mainly because Western and Central Alps are characterised by a small to moderate seismicity only.

In our results the expected normal regime dominating the Apennines is confirmed, all along the watershed (zones. n. 18, 19, 24, 33, 39, 45), following the typical tectonic style of the seismic sequences occurred in this narrow zone in the last tens of years, i.e. from north to south the 1997-1998 Umbria Marche, the 2016-2017 Central Italy, the 2009 L'Aquila and the 1980 Irpinia. In the outer part of the Apennines the style-of-faulting changes with depth and moving to east, to a reverse regime, sometime mixed with a strike-slip style, as in the zones n. 21, 26, 29, 34 and 36. The 3D approach we applied, allowed to detect the transition from normal to reverse with depth along the Northern and Central Apennines and to solve the abruptness of this transition given by a 2D approach only.

Along the peninsula, few seismic zones have a final 100% random source result and this occurs where the seismicity is really scarce and with small to moderate earthquakes (zones n. 22, 27, 28, 31, 37 and 38).

The seismic zones where however the strike-slip style of faulting mainly dominates are in Eastern Sicily, from the Aeolian Islands through the Etna volcano toward south up to the Iblei mountains (zones n. 44, 49, 48); this is not surprising considering that this N-S narrow band is interpreted aa the transfer zone between the Calabrian arc subduction system and the Sicily continental environment.

The robustness of these results is confirmed by their correspondence with the geological models and by the good comparison made with the most recent earthquakes occurred in Italy, independently from their magnitudes. Finally, these results are in use in the recent elaboration of a new seismic hazard model for Italy.

Competing interests

The authors declare that they have no conflict of interest.

485 **Data availability**

The dataset of focal mechanisms used for this study is included in the Supplement (see below). All results and data used to obtain them are reported in Tables in the text

Supplements

490 Table 1_Supplement — Depth parameters used for ZS16 seismic zones.
Table 2_Supplement — Dataset used in this study, gathering all seismic moment tensors used in this work, including also single earthquake information.

References

495 Allmendinger, R. W., Cardozo, N., and Fisher, D., 2012, Structural geology algorithms: Vectors and tensors in structural geology: Cambridge University Press, 302 p.

Anzidei, M., Maramai, A. and Montone, P. (eds): The Emilia (northern Italy) seismic sequence of May-June, 2012: preliminary data and results, Ann. of Geophysics, 55, 4, 515-
500 842, doi: 10.4401/ag-6232, 2012.

Akkar, S., M. A., Sandıkkaya and J. J. Bommer: Empirical ground-motion models for point- and extended-source crustal earthquake scenarios in Europe and the Middle East, Bull. Earthquake. Eng., 12:359–387, 10.1007/s10518-013-9461-4, 2014.

505
Bernardi, F., Braunmiller, J., Kradolfer, U. and Giardini, D.: Automatic regional moment tensor inversion in the European-Mediterranean region, Geophys. J. Int.,157, 703–716, 2004.

510 Bindi, D., Pacor, F., Luzi, L., Puglia, R., Massa, M., Ameri, G. and Paolucci, R.: Ground motion prediction equations derived from the Italian strong motion database, Bull. Earthquake Eng., 9, 1899–1920, https://doi.org/10.1007/s10518-011-9313-z, 2011.

Bindi, D., Massa, M., Luzi, L., Ameri, G., Pacor, F., Puglia, R. and Augliera, P.: Pan-
515 European ground-motion prediction equations for the average horizontal component of PGA, PGV, and 5 %-damped PSA at spectral periods up to 3.0 s using the RESORCE dataset. Bull Earthquake Eng 12, 391–430, https://doi.org/10.1007/s10518-013-9525-5, 2014.

Bommer, J.J., Douglas, J. and Strasser, F.O.: Style-of-Faulting in Ground-Motion Prediction
520 Equations, Bulletin of Earthquake Engineering 1, 171–203, https://doi.org/10.1023/A:1026323123154, 2003.

CMT Italian Dataset, http://rcmt2.bo.ingv.it/Italydataset.html, doi:10.13127/rcmt/italy, last access: 15 July 2020.
525
Chiarabba, C., De Gori, P., Cattaneo, M., Spallarossa, D. and Segou, M.: Faults geometry and the role of fluids in the 2016–2017 Central Italy seismic sequence, Geophysical Research Letters, 45, 6963– 6971, https://doi.org/10.1029/2018GL077485, 2018.

530   D'Agostino, N., D'Anastasio, E., Gervasi, A., Guerra, I., Nedimović, M.R., Seeber, L. and Steckler, M.: Forearc extension and slow rollback of the Calabria Arc from GPS measurements, Geophys. Res. Lett., 38, I17304, http://dx.doi.org/10.1029/2011GL048270, 2011.

535   DISS Working Group: Database of Individual Seismogenic Sources (DISS), Version 3.2.1: A compilation of potential sources for earthquakes larger than M 5.5 in Italy and surrounding areas, http://diss.rm.ingv.it/diss/, Istituto Nazionale di Geofisica e Vulcanologia, 10.6092/INGV.IT-DISS3.2.1, 2018, last access: 15 July 2020.

540   Dziewonski, A. M., Chou, T.-A. and Woodhouse, J. H.: Determination of earthquake source parameters from waveform data for studies of global and regional seismicity, J. Geophys. Res., 86, 2825-2852, doi: 10.1029/JB086iB04p02825, 1981.

    Ekström, G., Nettles, M. and Dziewonski, A. M.: The global CMT project 2004-2010:
545   Centroid-moment tensors for 13,017 earthquakes, Phys. Earth Planet. Inter., 200-201, 1-9, https://www.globalcmt.org, doi:10.1016/j.pepi.2012.04.002, 2012.

    European Mediterranean RCMT Catalog, http:\\www.bo.ingv.it/RCMT, doi:10.13127/rcmt/euromed, last access: 15 July 2020.
550

    Galadini, F. and P. Galli, P.: The Holocene paleo-earthquakes on the 1915 Avezzano earthquake faults (central Italy): implications for active tectonics in the central Apennines. Tectonophysics, 308,143-170, 1999.

555   Gasperini, P., Lolli, B., and Vannucci, G.: Relative frequencies of seismic main shocks after strong shocks in Italy, Geophysical Journal International, 207, 1, 150–159, https://doi.org/10.1093/gji/ggw263, 2016.

    ISIDe Working Group: Italian Seismological Instrumental and Parametric Database (ISIDe),
560   Istituto Nazionale di Geofisica e Vulcanologia (INGV), https://doi.org/10.13127/ISIDE, 2007, last access: 15 July 2020.

    Loreto, M.F., Fracassi, U., Franzo, A., Del Negro, P., Zgur, F., and Facchin, L.: Approaching the seismogenic source of the Calabria 8 September 1905 earthquake: New geophysical,
565   geological and biochemical data from the S. Eufemia Gulf (S Italy), Marine Geology, 343, 62-75, ISSN 0025-3227, https://doi.org/10.1016/j.margeo.2013.06.016, 2013.

    Marchetti, A. et al.: The Italian Seismic Bulletin: strategies, revised pickings and locations of the central Italy seismic sequence, Ann. of Geophysics, 59, DOI: 10.4401/ag –7169, 2016.
570

    Marrett, R. A., and Allmendinger, R. W.: Kinematic analysis of fault-slip data, J. of Structural Geology, v. 12, p. 973-986, 1990.

    Meletti, C., Galadini, F.,Valensise, G.,Stucchi, M., Basili, R., Barba, S., Vannucci, G. and
575   Boschi, E.: A seismic source model for the seimic hazard assessment of the Italian territory, Tectonophys., 85-108,10.1016/j.tecto.2008.01.003, 2008.

Meletti, C., Visini, F., D'Amico, V., Pace, B. and Rovida, A.: The seismicity model for Italy MA4. Internal report Seismic Hazard Center, 2019.

580

Meletti, C., Marzocchi, W. and MPS16 Working Group: The 2016 Italian seismic hazard model, in Proc. 16th World Conference on Earthquake Engineering, Santiago de Chile, January 9–13, 747, S-P1463070033, 2017.

585   Kostrov, V. V.: Seismic moment and energy of earthquakes and seismic flow of rocks, Izv. Acad. Sci. USSR, Phys. Solid Earth, 1, 23–40, 1974.

Pagani, M., Monelli, D., Weatherill, G., Danciu, L., Crow–ley, H., Silva, V., et al.: OpenQuake engine: An open hazard (and risk) software for the global earthquake model. Seismological
590   Research Letters, 85(3), 692–702. https://doi.org/10.1785/0220130087, 2014.

Pondrelli, S., Ekström, G. and Morelli, A.: Seismotectonic re-evaluation of the 1976 Friuli, Italy, seismic sequence, J. Seismology, 5(1), 73–83, https://doi.org/10.1023/a:1009822018837, 2001.

595

Pondrelli, S., Morelli, A., Ekström, G., Mazza, S., Boschi, E. and Dziewonski, A. M.: European-Mediterranean regional centroid-moment tensors: 1997-2000, Phys. Earth Planet. Int., 130, 71-101, 2002.

600   Pondrelli, S., Salimbeni, S., Ekström, G., Morelli, A., Gasperini, P. and Vannucci, G.: The Italian CMT dataset from 1977 to the present, Phys. Earth Planet. Int., doi:10.1016/j.pepi.2006.07.008,159/3-4, pp. 286-303, 2006.

Pondrelli, S. and Salimbeni, S.: Regional Moment Tensor Review: An Example from the
605   European Mediterranean Region. In Encyclopedia of Earthquake Engineering (pp. 1-15), http://link.springer.com/referenceworkentry/10.1007/978-3-642-36197-5_301-1, Springer Berlin Heidelberg, 2015.

Roselli, P., Marzocchi, W., Mariucci M. T. and Montone, P.: Earthquake focal mechanism
610   forecasting in Italy for PSHA purposes. Geophys. J. Int., 212, 491–508, doi: 10.1093/gji/ggx383, 2017.

Rovida, A., Locati, M., Camassi, R., Lolli, B., Gasperini, P. (eds): CPTI15, the 2015 version of the Parametric Catalogue of Italian Earthquakes. Istituto Nazionale di Geofisica e
615   Vulcanologia. doi:http://doi.org/10.6092/INGV.IT–CPTI15, 2016, last access: 15 July 2020.

Saul, J., Becker, J., Hanka, W.: Global moment tensor computation at GFZ Potsdam, AGU 2011 Fall Meeting, 2011.

620   Serpelloni, E., M. Anzidei, P. Baldi, G. Casula, A. Galvani: Crustal velocity and strain-rate fields in Italy and surrounding regions: new results from the analysis of permanent and non-permanent GPS networks, Geophysical Journal International, 161, 3, 861–880, https://doi.org/10.1111/j.1365-246X.2005.02618.x, 2005.

625   Stucchi, M., Meletti, C., Montaldo, V., Crowley, H., Calvi, G.M., and Boschi, E.: Seismic Hazard Assessment (2003–2009) for the Italian Building Code, Bull. Seismol. Soc. Am. 101, 4, 1885–1911, 2011.

Vannucci, G. and Gasperini, P.: The new release of the database of Earthquake
630   Mechanisms of the Mediterranean Area (EMMA Version 2), Annals of Geophysics, Suppl. V. 47, N.1, 307-334, 2004.

Wessel, P., & Smith, W. H. F. (1998). New, improved version of Generic Mapping Tools released. Eos, Transactions American Geophysical Union, 79(47), 579.
635   https://doi.org/10.1029/98EO00426

640

TABLES

Table 1 - Data for each seismic zone, including seismogenic thickness used for the summation of focal mechanisms, number of available focal mechanisms, cumulative M_{0sum} and cumulative focal mechanism for each tectonic style (NF, SS, TF). "s" and "d" added to the seismic zone number refer to shallow and deep zones, when the summation is done for different depth intervals.

N.	Seismic Zone	Thickness (km)	n. NF	NF M_{0sum} (dyn cm)	cumulative NF strike, dip, rake	n. SS	SS M_{0sum} (dyn cm)	cumulative SS strike, dip, rake	n. TF	TF M_{0sum} (dyn cm)	cumulative TF strike, dip, rake
1	Idria	0-40	—	—	—	7	3.86E+24	219, 67, -2	2	9.00E+22	—
2	Slovenia	0-40	—	—	—	3	1.18E+24	135, 68, 160	3	1.70E+23	131, 25, 66
3	Friuli	0-40	—	—	—	13	1.01E+25	293, 86, -178	16	8.14E+25	274, 25, 112
4	Valtellina - Alto Adige	0-40	—	—	—	2	5.50E+23	—	1	1.46E+23	—
5	Innsbruck	0-40	—	—	—	1	7.03E+23	—	—	—	—
6	Grigioni	0-40	4	1.00E+24	295, 38, -77	1	1.12E+23	—	—	—	—
7	Garda-Soncino	0-40	1	1.27E+23	—	2	6.50E+23	—	3	4.70E+23	234, 26, 90
8	Montreux	0-40	1	—	—	—	—	—	—	—	—
9	Vallese	0-40	—	—	—	7	9.10E+23	102, 25, -107	—	—	—
10	Western Alps	0-40	4	3.40E+23	284, 37, -89	9	4.47E+24	310, 15, -32	—	—	—
11	Piemonte	0-40	1	2.26E+23	—	7	1.73E+24	222, 74, -164	2	2.00E+22	—
12	Mantova Verona	0-40	—	—	—	4	7.80E+23	104, 60, -150	2	2.50E+23	—
13	Pianura veneta	0-40	—	—	—	—	—	—	—	—	—
14	Imperiese	0-40	1	3.27E+23	—	1	1.12E+23	—	2	1.48E+23	—
15	Mar Ligure	0-40	—	—	—	3	6.50E+23	264, 57, 169	3	1.35E+25	220, 45, 123
16	Tortona-Bobbio	0-40	2	1.50E+23	—	7	9.70E+23	110, 36, -135	2	5.00E+22	—
17	Spezia North of Tuscany	0-40	2	1.20E+23	—	5	3.10E+23	88, 67, -172	1	2.28E+22	—
18	Lunigiana-Casentino	0-40	11	1.17E+24	308, 35, -90	6	3.40E+24	288, 35, -118	—	—	—
19s	Tuscany-Emilia Apennines Shallow	0-15	7	3.30E+23	309, 44, -99	3	2.30E+23	342, 39, -45	2	9.00E+22	—
19d	Tuscany-Emilia Apennines Deep	15.1-40	1	1.10E+23	—	2	1.20E+23	—	4	3.20E+24	278, 34, 84
20s	Emilia Shallow	0-20	—	—	—	1	1.44E+22	—	11	7.80E+23	299, 36, 87
20d	Emilia Deep	20.1-40	—	—	—	3	6.20E+23	9, 38, 26	—	—	—

#	Region	Depth	N	M	Plane	N	M	Plane	N	M	Plane
21	Ferrara Arc	0-40	—	—	—	9	7.2E+23	40, 66, 16	17	3.26E+25	90, 33, 66
22	Geothermal reg. Tuscany Latium	0-40	—	—	—	—	—	—	—	—	—
23	Trasimeno-Southern Latium	0-40	—	—	—	4	2.2E+23	228, 3, 64	—	—	—
24	Umbria-Abruzzo	0-40	89	2.18E+26	321, 37, -86	15	3.47E24	164, 31, -65	—	—	—
25s	Inner part of Marche	0-12.5	2	6.60E+23		2	4.05E24		—	—	—
25d	Inner part of Marche	12.6-40	—	—	—	5	2.00E23	104, 76, -176	1	6.00E+22	—
26	Rimini-Conero-Majella	0-40	—	—	—	9	1.40E+24	117, 49, 15	5	8.10E+23	112, 38, 61
27	Northern Tyrrhenian Coast	0-40	—	—	—	1	1.77E23	—	—	—	—
28	Colli Albani	0-40	—	—	—	—	—	—	—	—	—
29	Chieti-Pescara	0-40	—	—	—	2	6.00E22	—	4	2.90E+23	191, 44, 64
30	Central Adriatic Sea	0-40	1	3.44E+23	—	3	1.39E+24	267, 71, -9	18	5.73E+24	286, 44, 92
31	Ischia-Vesuvio	0-40	—	—	—	—	—	—	—	—	—
32	Campania part of the Tyrrhenian coast	0-40	1	2.48E+25	—	2	5.20E+23	—	—	—	—
33	Sannio-Irpinia	0-40	20	2.57E+26	135, 40, -80	3	5.12E+24	190, 42, -39	—	—	—
34	Gargano	0-40	—	—	—	11	1.03E+25	176, 73, 0	4	8.80E+23	205, 33, 66
35	Ofanto	0-40	3	1.41E+25	168, 31, -55	5	1.40E+25	163, 67, 171	—	—	—
36	Potenza-Matera	0-40	1	8.47E+22	—	5	6.49E+24	184, 73, 10	—	—	—
37	Southern Puglia	0-40	—	—	—	—	—	—	—	—	—
38	Otranto channel	0-40	—	—	—	1	6.00E+23	—	—	—	—
39	Calabrian part of the Tyrrhenian coast	0-40	7	6.49E+26	358, 39, -113	4	4.10E+23	331,61, 171	—	—	—
40	Calabrian part of the Ionian coast	0-40	1	8.36E+23	—	5	4.76E+24	300, 64, -165	2	1.40E+23	—
41	Ionian Sea	0-40	—	—	—	11	5.37E+24	278, 59, 171	2	2.30E+23	—
42	Sardegna-Corsica	0-40	—	—	—	1	2.94E+22		8	2.93E+24	237, 34, 87
43	Ustica-Alicudi	0-40	—	—	—	3	1.16E+25	24, 45, 41	21	9.03E+24	72, 38, 90

44	Eolie-Patti	0-40	4	2.70E+23	16, 32, -105	9	1.50E+25	135, 60, -176	3	2.20E+23	294, 32, 96
45	Cefalù	0-40	5	5.70E+23	100, 36, -111	7	1.87E+24	21, 14, -148	—	—	—
46	Western Sicily	0-40	—	—	—	6	1.15E+25	268, 50, 33	1	3.09E+23	—
47	Malta Lampedusa	0-40	1	2.51E+22	—	9	2.79E+24	189, 70, -5	2	7.00E+23	—
48	Iblei	0-40	—	—	—	3	3.60E+23	190, 80, 4	1	5.54E+22	—
49	Etna	0-40	—	—	—	8	4.60E+23	46, 68, 20			—
50	Southern Tyrrhenian Sea	0-40	3	1.31E+24	18, 35, -111	4	s	253, 11, -29	1	4.33E+23	—

650

Table 2 - Results of the evaluation of P-, T- and B- axis dispersion. In each column is reported Δ, in degrees, i.e. the median of the angular differences between the axes of each single focal mechanism and the axes of the cumulative one (see Figure 4).

N.	Seismic Zone	Δ NF T-axes	Δ NF B-axes	Δ NF P-axes	Δ SS T-axes	Δ SS B-axes	Δ SS P-axes	Δ TF T-axes	Δ TF B-axes	Δ TF P-axes
1	Idria	—	—	—	29	26	18	29	26	18
2	Slovenia	—	—	—	25	24	1	6	31	32
3	Friuli	—	—	—	43	44	2	13	13	14
4	Valtellina - Alto Adige	—	—	—	—	—	—	—	—	—
5	Innsbruck	—	—	—	—	—	—	—	—	—
6	Grigioni	41	44	9	41	44	9	41	44	9
7	Garda-Soncino	—	—	—	—	—	—	31	24	23
8	Montreux	—	—	—	—	—	—	—	—	—
9	Vallese	—	—	—	30	59	56	30	59	56
10	Western Alps	43	50	22	5	8	61	5	8	61
11	Piemonte	—	—	—	5	26	34	2	19	7
12	Mantova-Verona	—	—	—	34	29	15	34	29	15
13	Pianura veneta	—	—	—	—	—	—	—	—	—
14	Imperiese	—	—	—	—	—	—	—	—	—
15	Mar Ligure	—	—	—	22	24	19	14	1	18
16	Tortona-Bobbio	—	—	—	32	68	78	32	68	78
17	Spezia-North of Tuscany	—	—	—	22	4	18	22	4	18
18	Lunigiana-Casentino	12	19	18	26	35	45	26	35	45
19s	Tuscany-Emilia Apennines Shallow	3	3	19	29	28	27	6	5	6
19d	Tuscany-Emilia Apennines Deep	1	0	0	14	14	17	6	9	8
20s	Emilia Shallow	—	—	—	—	—	—	13	16	11
20d	Emilia Deep	—	—	—	15	12	11	15	12	11
21	Ferrara Arc	—	—	—	25	31	20	15	19	12
22	Geothermal reg. Tuscany Latium	—	—	—	—	—	—	—	—	—
23	Trasimeno-Southern Latium	—	—	—	9	9	7	9	9	7
24	Umbria-Abruzzo	18	19	18	29	41	53	29	41	53
25s	Inner part of Marche	2	3	2	4	4	8	4	4	8
25d	Inner part of Marche	—	—	—	38	32	3		5	2
26	Rimini-Conero-Majella	—	—	—	37	47	27	17	2	13
27	Northern Tyrrhenian Coast	—	—	—	—	—	—	—	—	—
28	Colli Albani	—	—	—	—	—	—	—	—	—
29	Chieti-Pescara	—	—	—				12	12	1
30	Central Adriatic Sea	—	—	—	29	18	25	19	21	18
31	Ischia-Vesuvio	—	—	—	—	—	—	—	—	—

32	Campania part of Tyrrhenian coast	—	—	—	5	42	1	5	42	1
33	Sannio-Irpinia	2	22	21	82	49	62	82	49	62
34	Gargano				24	33	16	23	21	23
35	Ofanto	20	17	13	82	24	84	82	24	84
36	Potenza-Matera	—	—	—	13	30	16	13	30	16
37	Southern Puglia	—	—	—	—	—	—	—	—	—
38	Otranto channel	—	—	—	0	1	—	0	1	—
39	Calabrian part of Tyrrhenian coast	3	25	3	26	34	22	26	34	22
40	Calabrian part of Ionian coast	—	—	—	74	22	56	74	22	56
41	Ionian Sea	—	—	—	36	30	3	36	30	3
42	Sardegna-Corsica	—	—	—	—	—	—	16	48	47
43	Ustica-Alicudi	—	—	—	57	18	20	14	16	16
44	Eolie-Patti	8	6	8	56	48	39	2	25	30
45	Cefalù	16	17	22	27	48	4	27	48	4
46	Western Sicily	—	—	—	17	13	12	17	13	12
47	Malta-Lampedusa	—	—	—	25	20	32	25	20	32
48	Iblei	—	—	—	24	19	11	24	19	11
49	Etna	—	—	—	40	28	5	40	28	5
50	Southern Tyrrhenian Sea	49	45	17	24	22	20	24	22	20

660 Table 3 - Final style-of-faulting for each seismic zone, with the total amount of used focal mechanisms, the total released seismic moment M_{0Total} per zone and the percentage of contribution of each tectonic style to the final source.

N.	Seismic Zone Name	n. of focal mec.	M_{0Total} (dyn cm)	%NF	%SS	%TF	Final Style-of-faulting
1	Idria	9	3.94E+24	0	98	2	SS100%
2	Slovenia	6	1.35E+24	0	87	13	SS85% + TF15%
3	Friuli	29	9.15E+25	0	11	89	TF90% + SS10%
4	Valtellina - Alto Adige	3	6.96E+23	0	79	21	SSrand80% + TFrand20%
5	Innsbruck	1	—	—	—	—	random 100%
6	Grigioni	5	1.11E+24	90	10	0	NF100%
7	Garda-Soncino	6	1.25E+24	10	52	38	SSrand60%+TFrand40% (100%rand)
8	Montreux	1	—	—	—	—	random 100%
9	Vallese	7	9.10E+23	0	100	0	SSrand100%
10	Western Alps	13	4.81E+24	7	93	0	SSrand100%
11	Piemonte	10	1.98E+24	11	88	1	NFrand10% + SSrand90%
12	Mantova-Verona	6	1.03E+24	0	76	24	SS75% + TFrand25%
13	Pianura veneta	0	—	—	—	—	random 100%
14	Imperiese	4	5.87E+23	56	19	25	random100%
15	Mar Ligure	6	1.42E+25	0	5	95	TF100%
16	Tortona-Bobbio	11	1.17E+24	13	83	4	NFrand15% + SSrand85%
17	Spezia-North of Tuscany	8	4.53E+23	27	68	5	SS70% + NFrand30%
18	Lunigiana-Casentino	17	4.57E+24	26	74	0	NF30% + SSrand70%
19s	Tuscany-Emilia Apennines Shallow	12	6.50E+23	51	35	14	NF50% + SS35% + TFrand15%
19d	Tuscany-Emilia Apennines Deep	7	3.43E+24	3	3	93	TF100%
20s	Emilia Shallow	12	7.94E+23	0	2	98	TF100%
20d	Emilia Deep	3	6.20E+23	0	100	0	SS100%
21	Ferrara Arc	26	3.33E+25	0	2	98	TF100%
22	Geothermal reg. Tuscany Latium	0	—	—	—	—	random 100%
23	Trasimeno Southern Latium	4	2.20E+23	0	100	0	SSrand100%
24	Umbria-Abruzzo	104	2.22E+26	98	2	0	NF100%

25s	Inner part of Marche	4	4.71E+24	14	86	0	SSrand85% + NFrand15%
25d	Inner part of Marche	6	2.60E+23	0	77	23	SSrand75% + TFrand25%
26	Rimini-Conero Majella	14	2.21E+24	0	63	37	TF40% + SSrand 60%
27	Northern Tyrrhenian Coast	1	—	—	—	—	random 100%
28	Colli Albani	0	—	—	—	—	random 100%
29	Chieti-Pescara	6	3.50E+23	0	17	83	TF80% + SSrand20%
30	Central Adriatic Sea	22	7.46E+24	5	19	77	TF80% + SS20%
31	Ischia-Vesuvio	0	—	—	—	—	random 100%
32	Campania part of Tyrrhenian coast	3	2.53E+25	98	2	0	NFrand100%
33	Sannio-Irpinia	23	2.62E+26	98	2	0	NF100%
34	Gargano	15	1.12E+25	0	92	8	SS100%
35	Ofanto	8	2.81E+25	50	50	0	NF50%+SSrand50%
36	Potenza-Matera	6	6.57E+24	1	99	0	SS100%
37	Southern Puglia	0	—	—	—	—	random 100%
38	Otranto channel	1	—	—	—	—	random 100%
39	Calabrian part of Tyrrhenian coast	11	6.50E+26	100	0	0	NF100%
40	Calabrian part of Ionian coast	8	5.74E+24	15	83	2	NFrand15% + SSrand85%
41	Ionian Sea	13	5.60E+24	0	96	4	SS100%
42	Sardegna-Corsica	9	2.96E+24	0	1	99	TF ran 100%
43	Ustica-Alicudi	24	2.06E+25	0	56	44	TF45%+SS55%
44	Eolie-Patti	16	1.55E+25	2	97	1	SSrand100%
45	Cefalù	12	2.44E+24	23	77	0	NF25% + SSrand75%
46	Western Sicily	7	1.18E+25	0	97	3	SS100%
47	Malta-Lampedusa	12	3.52E+24	1	79	20	SS80% + TFrand20%
48	Iblei	4	4.15E+23	0	87	13	SS90% + TFrand10%
49	Etna	8	4.60E+23	0	100	0	SS100%
50	Southern Tyrrhenian Sea	8	2.49E+24	53	30	17	NFrand50%+ SS30% + TFrand20%

665

Table 4 — List of earthquakes occurred after 2015, used in the comparison with the results of this study.

ID event	Date (yyyy-mm-dd)	Time UTC	Lat	Long	Depth (km)	Mw
1	2016-02-08	15:35:43.39	36.97	14.86	7.4	4.2
2	2016-08-24	01:36:32.00	42.69	13.23	8.1	6.0
3	2016-10-30	06:40:17.32	42.83	13.10	10.0	6.5
4	2017-01-18	10:14:09.90	42.53	13.28	9.6	5.5
5	2017-02-03	04:10:05.32	42.99	13.01	7.1	4.2
6	2017-11-19	12:37:44.70	44.66	10.03	22.4	4.4
7	2018-04-10	03:11:30.76	43.06	13.03	8.1	4.6
8	2018-08-14	21:48:30.98	41.88	14.84	19.2	4.6
9	2018-08-16	18:19:04.60	41.87	14.86	19.6	5.1
10	2018-10-06	00:34:19.79	37.60	14.93	4.5	4.6
11	2018-12-26	02:19:14.00	37.64	15.11	10.0	4.9
12	2019-01-14	23:03:57.02	44.34	12.28	20.6	4.3

670

675

FIGURES and CAPTIONS
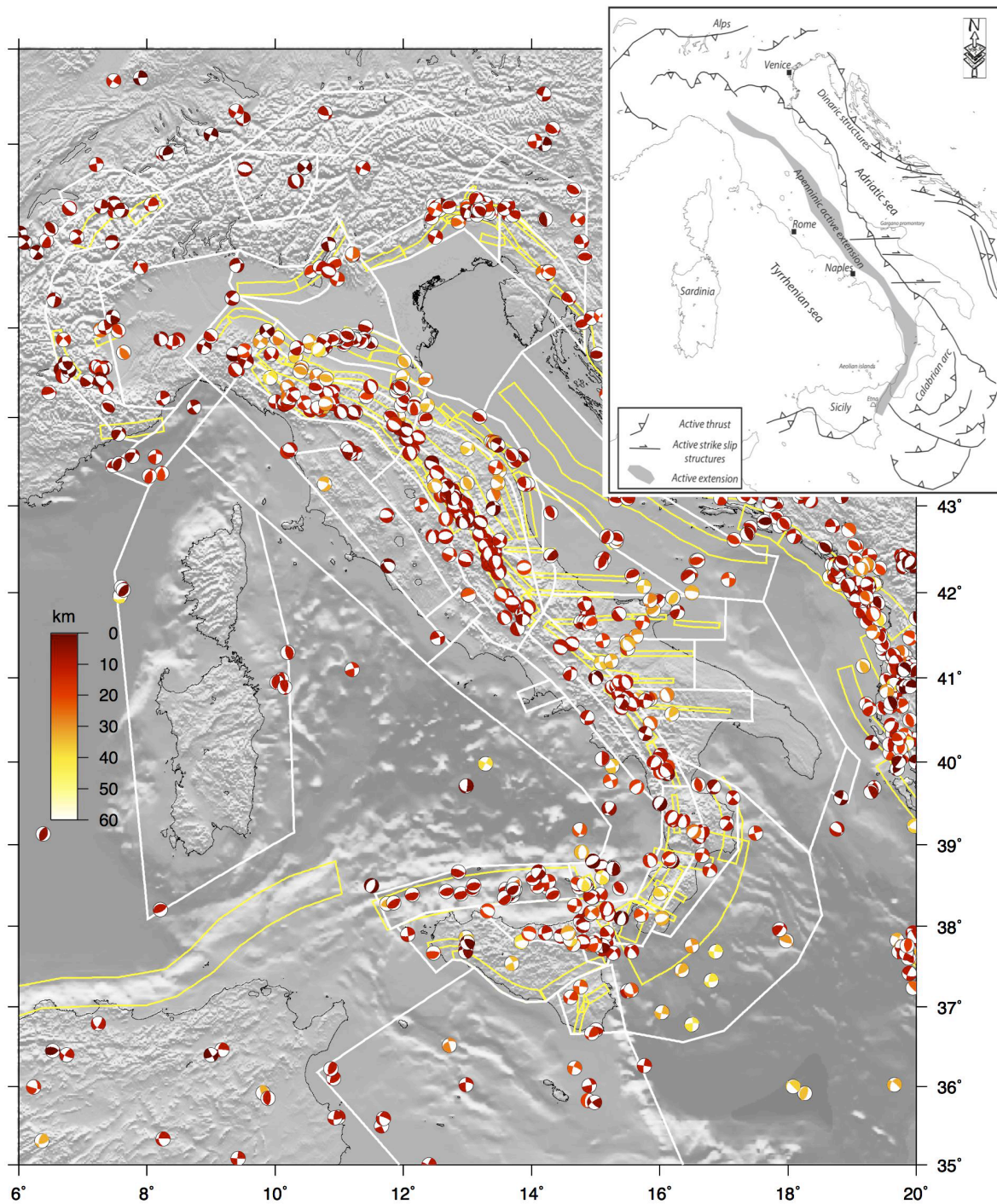
Figure 1 - Map of the entire available dataset. Different colors of the focal mechanisms represent different hypocentral depths, following the scale on the left. On the background, the borders of the seismic source zones of ZS16 (Meletti et al., 2019) are reported in white; in yellow, Composite Seismogenic Sources taken from DISS database (DISS Working Group, 2018; http://diss.rm.ingv.it/diss). Top right, map of main tectonic features of the study region.
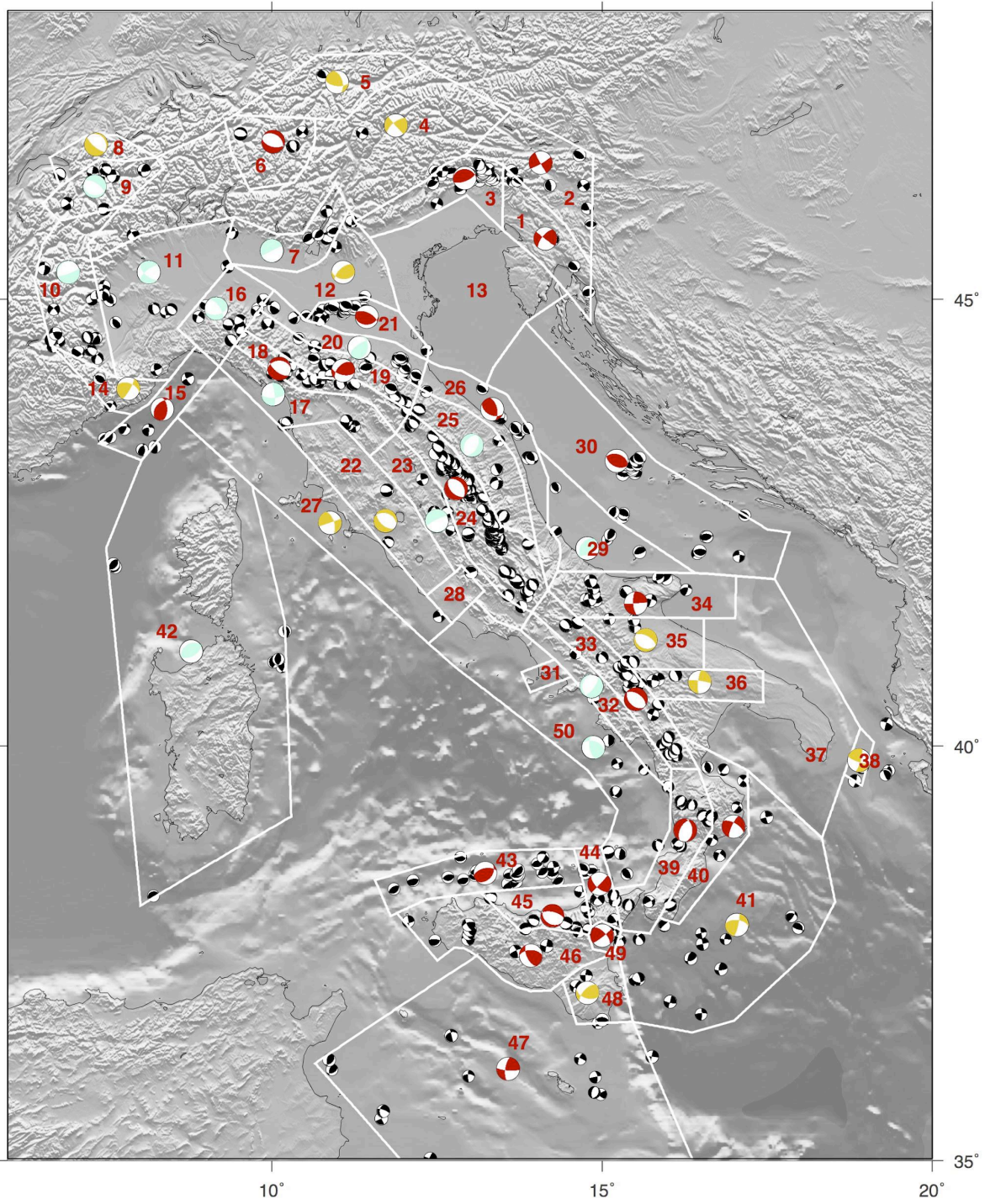
690

Figure 2 - Map of the results of a test of focal mechanisms summation for each seismic zone in ZS16 (contoured in white, numbered in red) using a 20 km seismogenic layer thickness. Obtained cumulative focal mechanisms are in red when considered a stable result, yellow when less reliable, light blue when too uncertain because of the heterogeneity of input data

695 (see in the text for quality evaluation criteria). On the background, the small black focal mechanisms are the input dataset.
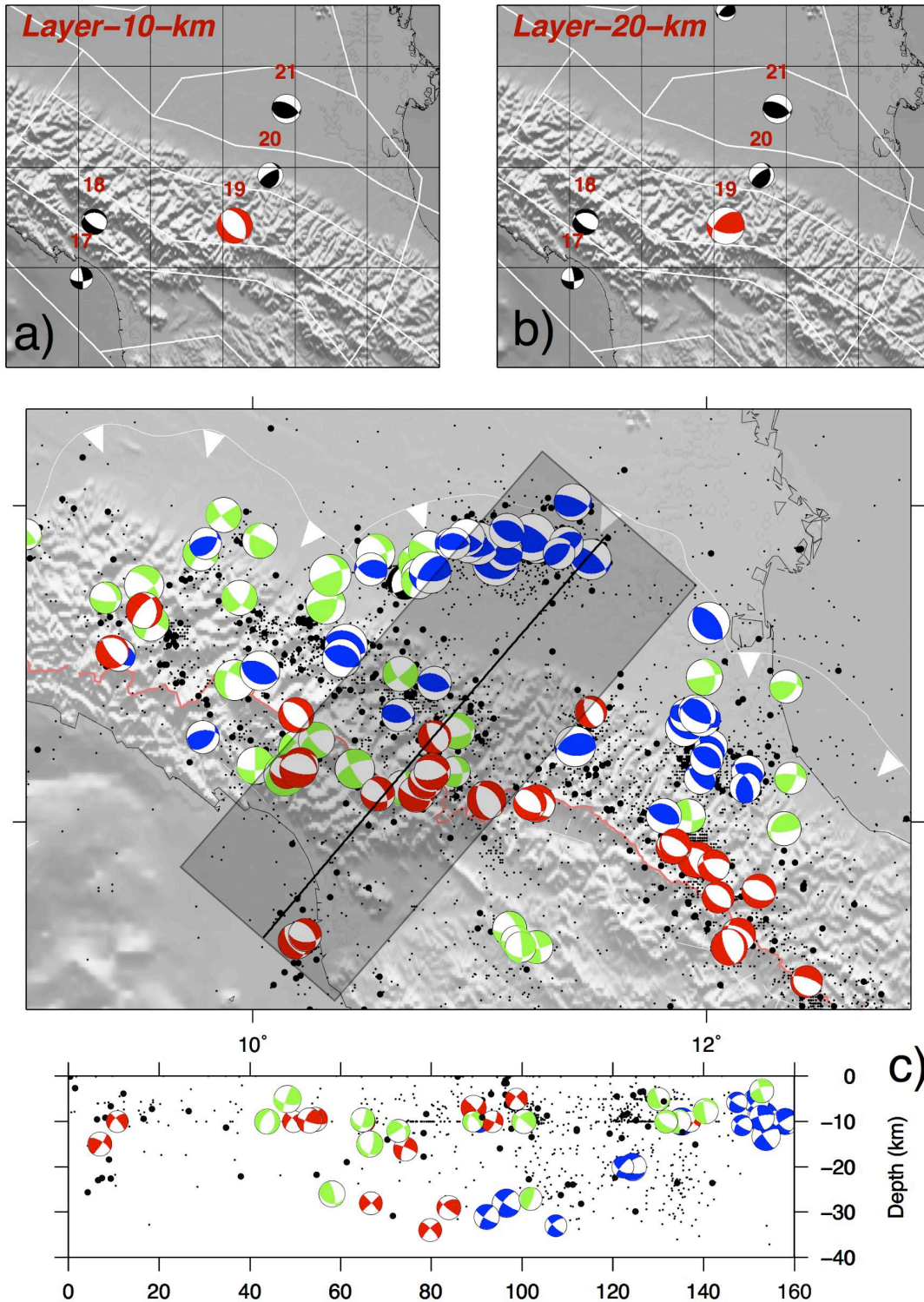
Figure 3 - a) and b) are an example of tectonic style layering, for the seismic zone n. 19. The cumulative moment tensor obtained for 10 km of thickness shows a completely different result with respect to the one given by 20 km. Red numbers indicate the seismic zones. c) map and section of our dataset in the region of the seismic zone n.19; red, green and blue focal mechanisms are respectively normal, strike-slip and reverse type. Seismicity in the background (black dots, smaller are for events with M<3) is from ISIDe Working Group. (2007)
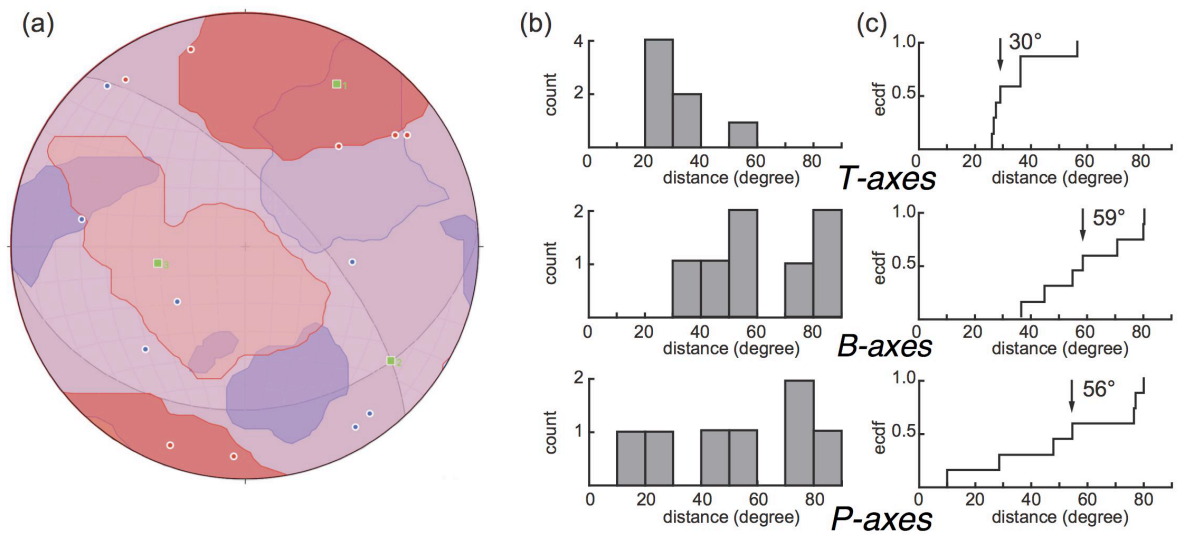
710

Figure 4 - An example of dispersion analysis for data of the seismic zone n.9. a) the possible cumulative focal mechanism obtained with the summation of all focal mechanisms available for this zone, all strike slip. Blue and red circles are P- and T- axes of input focal mechanisms, green symbols are P-, T- and B- axes of the cumulative one; blue and red

715 areas are P- and T- axes contours. b) histograms and c) cumulative curve of the angular difference between T- (top), B- (middle) and P- (bottom) axes of input and cumulative focal mechanisms. c) cumulative plots. Black arrows: median value.
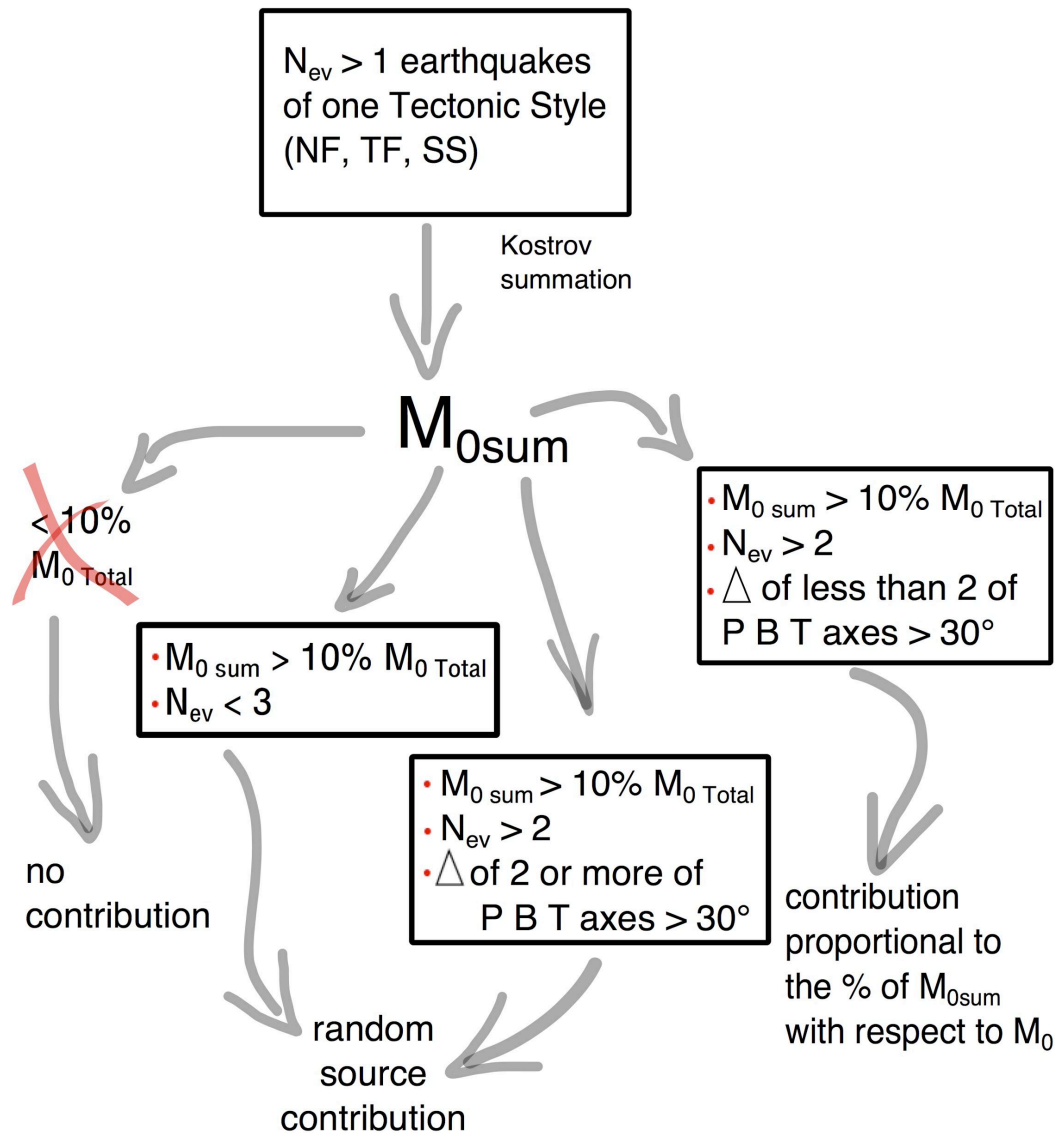
Figure 5 - Sketch of the decision making process applied to each zone and to each tectonic style group of earthquakes. N_{ev} is the number of available earthquakes; M_{0sum} is the seismic moment obtained summing the N_{ev} M_0; M_{0Total} is the cumulative seismic moment release in the singular zone independently from the tectonic style of events; Δ is the angular distance between P-, T- and B- axes of single focal mechanism involved in the summation and those of the cumulative one.
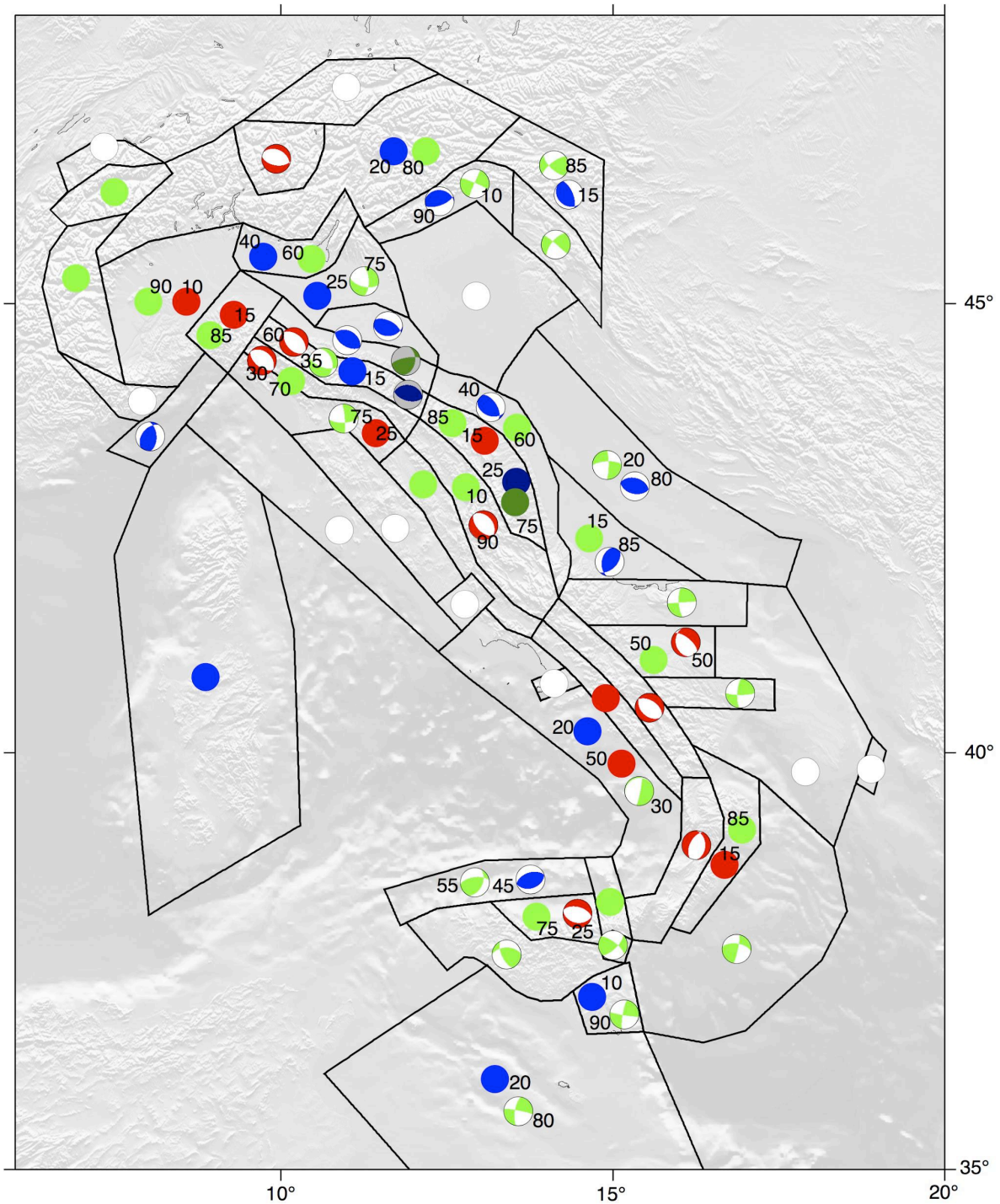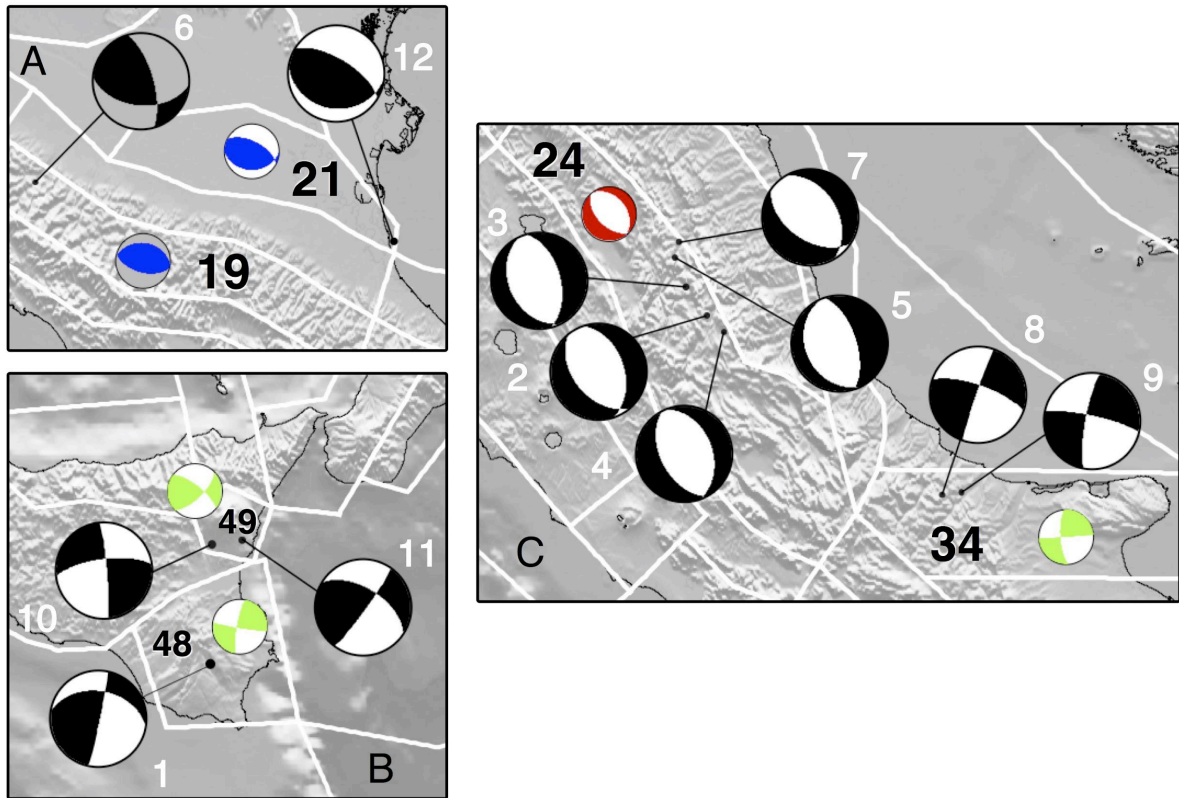
Figure 6 - Map of the expected style-of-faulting obtained for each seismic zone. Full circles represent random seismic sources: white circles are 100% random; blue, red and green circles are reverse, normal and strike-slip random sources, respectively. Same colors refer also to cumulative focal mechanisms. Focal mechanisms with a grey background or circles with darker colors represent the sources for deeper layers. Numbers in black are the percentage of contribution to the final source when it is composed by different styles.

Figure 7 — Comparison of seismic moment tensors of earthquakes occurred after 2015 (in black, see Table 4) and the expected style-of-faulting identified in the same seismic zone (for colors see Figure 6): A - Northern Apennines; B - Eastern Sicily; C - Central and Southern Apennines. Focal mechanisms with a grey background belong to deeper sources. Black numbers indicate the seismic zones, while black numbers refer to seismic events listed in Table 4.